## 1 The Physiological Basis for Estimating Photosynthesis from Chlorophyll a Fluorescence

- 2 Jimei Han<sup>1\*</sup>, Christine Y-Y. Chang<sup>1,2</sup>, Lianhong Gu<sup>3</sup>, Yongjiang Zhang<sup>4</sup>, Eliot W Meeker<sup>5</sup>,
- 3 Troy S. Magney<sup>6</sup>, Anthony P. Walker<sup>3</sup>, Jiaming Wen<sup>1</sup>, Oz Kira<sup>1,7</sup>, Sarah McNaull<sup>8</sup>, Ying Sun<sup>1\*</sup>

#### 4 ORCID

- 5 Jimei Han: <a href="https://orcid.org/0000-0001-7466-8511">https://orcid.org/0000-0001-7466-8511</a>
- 6 Christine Y-Y. Chang: https://orcid.org/0000-0001-6609-3527
- 7 Lianhong Gu: https://orcid.org/0000-0001-5756-8738
- 8 Yongjiang Zhang: <a href="https://orcid.org/0000-0001-5637-3015">https://orcid.org/0000-0001-5637-3015</a>
- 9 Troy S. Magney: <a href="https://orcid.org/0000-0002-9033-0024">https://orcid.org/0000-0002-9033-0024</a>
- 10 Anthony P. Walker: <a href="https://orcid.org/0000-0003-0557-5594">https://orcid.org/0000-0003-0557-5594</a>
- 11 Jiaming Wen: <a href="https://orcid.org/0000-0001-9840-0720">https://orcid.org/0000-0001-9840-0720</a>
- 12 Oz Kira: https://orcid.org/0000-0002-1620-2323
- 13 Ying Sun: <a href="https://orcid.org/0000-0002-9819-1241">https://orcid.org/0000-0002-9819-1241</a>
- 15 <sup>1</sup>School of Integrative Plant Science, Soil and Crop Science Section, Cornell University, Ithaca,
- 16 NY 14850, USA
- <sup>2</sup>USDA, Agricultural Research Service, Adaptive Cropping Systems Laboratory, Beltsville, MD
- 18 20705, USA

14

- <sup>3</sup>Environmental Sciences Division and Climate Change Science Institute, Oak Ridge National
- 20 Laboratory, Oak Ridge, Tennessee 37831, USA
- <sup>4</sup>School of Biology and Ecology, University of Maine, Orono, ME 04469, USA
- <sup>5</sup>Department of Chemical Engineering, University of California, Davis, CA 95616, USA
- <sup>6</sup>Department of Plant Sciences, University of California, Davis, CA 95616, USA
- <sup>7</sup>Department of Civil and Environmental Engineering, Ben-Gurion University of the Negev
- 25 8410501, Israel

- <sup>8</sup>Cornell Botanic Gardens, Cornell University, Ithaca, NY 14850, USA
- \*Corresponding to: <u>jh2757@cornell.edu</u> (J. Han), <u>ys776@cornell.edu</u> (Y. Sun)
- 29 This manuscript has been co-authored by UT-Battelle, LLC under Contract No. DE-AC05-00OR22725 with the U.S.
- 30 Department of Energy. The United States Government retains and the publisher, by accepting the article for
- 31 publication, acknowledges that the United States Government retains a non-exclusive, paid-up, irrevocable, worldwide

- 32 license to publish or reproduce the published form of this manuscript, or allow others to do so, for United States
- 33 Government purposes. The Department of Energy will provide public access to these results of federally sponsored
- research in accordance with the DOE Public Access Plan (<a href="http://energy.gov/downloads/doe-public-access-plan">http://energy.gov/downloads/doe-public-access-plan</a>).

## **Summary**

- The availability of Solar-Induced chlorophyll Fluorescence (SIF) offers potential to curb large uncertainties in estimating photosynthesis across biomes, climates, and scales. However, it remains unclear how SIF should be used to mechanistically estimate photosynthesis.
- This study built a quantitative framework to estimate photosynthesis, based on a mechanistic light reaction model with chlorophyll a fluorescence from PSII (*SIF*<sub>PSII</sub>) as an input (MLR-SIF). Utilizing 29  $C_3$  and  $C_4$  plant species representative of major plant biomes across the globe, we verified such a framework at the leaf level.
- MLR-SIF is capable of accurately reproducing photosynthesis for all  $C_3$  and  $C_4$  species under diverse light, temperature, and  $CO_2$  conditions. We further tested the robustness of MLR-SIF using Monte Carlo simulations, and found that the estimated photosynthesis is much less sensitive to parameter uncertainties relative to the conventional Farquhar, von Caemmerer, Berry (FvCB) model because of additional independent information contained in  $SIF_{PSII}$ .
- *SIF*<sub>PSII</sub>, once inferred from direct observables of SIF, provides "parameter savings" to the MLR-SIF as compared to the mechanistically equivalent FvCB and thus shortcuts the uncertainties propagated from imperfect model parameterization. Our findings set the stage for future efforts employing SIF mechanistically to improve photosynthesis estimation across scales, functional groups, and environmental conditions.

- **Key words:** photosynthesis model; Solar-induced chlorophyll Fluorescence (SIF); Non-
- Photochemical Quenching (NPQ); parameter uncertainty; redox state of PSII reaction centers
- 59 One Sentence Summary: Utilizing joint chlorophyll a fluorescence and gas exchange
- 60 measurements across diverse plant biomes, we build the physiological foundation for employing
- 61 SIF to mechanistically estimate photosynthesis.

#### Introduction

Accurate quantification of terrestrial photosynthesis at different spatiotemporal scales is a long-sought goal in carbon cycle science (Schimel, 1995; Beer *et al.*, 2010; Ciais *et al.*, 2014). The rapidly growing, cross-scale observational capability of Solar-Induced chlorophyll Fluorescence (SIF), the only optically detectable signal that probes the whole photosynthetic process (Porcar-Castell *et al.*, 2014), offers a promising opportunity to achieving the goal of quantifying photosynthesis across different spatiotemporal scales (Mohammed *et al.*, 2019; Porcar-Castell *et al.*, 2021). This has been evident by the dramatic growth of SIF research and efforts to transform SIF observations to terrestrial photosynthesis estimation over the last few decades (Mohammed *et al.*, 2019). However, how exactly SIF should be used to estimate photosynthetic carbon assimilation in natural environments remains elusive.

Initial findings have identified encouraging linkages between SIF and photosynthesis from both observational and modeling aspects. From the observational side, existing studies have empirically linked remotely sensed SIF with photosynthesis inferred from eddy covariance (EC) measurements of net ecosystem exchange (NEE) of CO<sub>2</sub> (e.g., Guanter et al., 2014; Joiner et al., 2014; Yang et al., 2015; Verma et al., 2017; Sun et al., 2017; Wood et al., 2017; Liu et al., 2017; Li et al., 2018; Miao et al., 2018; Yang et al., 2018). However, photosynthesis inferred from NEE at EC towers, although often assumed as the observational "truth", is not directly measured but indirectly and imprecisely derived with approaches known to contain errors or even biases (Wohlfahrt & Gu, 2015; Wehr et al., 2016; Keenan et al., 2019). Using potentially and likely biased estimates of photosynthesis as truth to infer SIF-photosynthesis relationships essentially contradicts the original motivation of applying SIF to constrain photosynthesis (or reduce uncertainties in photosynthesis estimates). Furthermore, it is circular to apply such SIF-photosynthesis relationships to back-calculate photosynthesis; this circular estimation does not fully take advantage of the mechanistic, independent information carried in SIF.

Existing modelling studies (e.g., Zhang et al., 2014; Koffi et al., 2015; Verrelst et al., 2016; Parazoo et al., 2020) primarily adopt the leaf-level formulation of the SIF-photosynthesis relationship from the SCOPE (Soil Canopy Observation Photosynthesis Energy) model (van der Tol et al., 2014). Specifically, this approach utilized the Farquhar, von Caemmerer, Berry (FvCB) biochemical model to compute photosynthesis (and photochemical quantum yield,  $\Phi_P$ ) (Farquhar et al., 1980; Sharkey, 1985). The modeled photosynthesis in turn is used to calculate fluorescence

yield ( $\Phi_F$ ) and therefore SIF by empirically modeling non-photochemical quenching (NPQ) as an exclusive function of  $\Phi_P$ . Terrestrial biosphere models (TBMs) that explicitly incorporate SIF and data assimilation systems that have adopted such formulations to ingest satellite SIF to improve photosynthesis (and net carbon budgets) estimates (*e.g.*, Thum *et al.*, 2017; Bacour *et al.*, 2019; Norton *et al.*, 2019). While useful for simulating SIF-photosynthesis relationships and their sensitivity to different environmental conditions, the SCOPE-based strategy cannot escape from the usual, well-known problems of parameter and scaling uncertainty in applying FvCB to estimate photosynthesis at scales beyond a leaf (*e.g.*, Rogers *et al.*, 2017; Schaefer *et al.*, 2012; Anav *et al.*, 2015). Indeed, Parazoo *et al.* (2020) reported wide discrepancies in modeled SIF and photosynthesis across TBMs and large disagreement with ground observations.

94

95

96

97

98

99

100

101

102

103

104

105

106

107

108

109

110

111

112

113

114

115

116

117

118

119

120

121

122

123

124

Moving forward, with emerging interest in taking advantage of the information contained in remotely sensed SIF observations to improve photosynthesis estimates, it is critical to develop a mechanistic approach that enables direct and independent estimation of photosynthesis from SIF. Photosynthesis consists of light and carbon (also known as dark, light-independent, or Calvin-Benson cycle) reactions in sequence, which collaborate via multiple feedforward and feedback mechanisms to ensure the safety and smooth operations of the photosynthetic machinery in dynamic environments (Rochaix, 2011; Roach & Krieger-Liszkay, 2014). SIF is emitted during the light reactions. The mechanistic light reaction (MLR) equations derived by Gu et al. (2019) established the theoretical relationship between SIF<sub>PSII</sub> (i.e., the true total chlorophyll a fluorescence - ChlF emitted from PSII, prior to signal attenuation due to leaf self-absorption) and the actual electron transport rate  $(J_a)$  from photosystem II (PSII) to photosystem I (PSI). Thus, if SIF is observed,  $J_a$  can be calculated, provided that the followings are known: 1) the escape probability, i.e., the ratio of the physiologically determined SIF<sub>PSII</sub> to the sensor-observed SIF, which can be determined via leaf/canopy/atmosphere radiative transfer modeling (e.g., Yang & van der Tol, 2018; Liu et al., 2019; Zeng et al., 2019), and 2) either the fraction of open PSII reaction centers  $(q_L)$  or NPQ (only one is needed as the other can be resolved with  $SIF_{PSII}$ ; Gu et al., 2019). Photosynthesis can then be determined from the rates of carboxylation and photorespiration that the SIF-informed  $J_a$  supports (Farguhar et al., 1980; Sharkey, 1985; Blankenship, 2002; von Caemmerer, 2000). Photosynthesis estimated from observed SIF is based upon theory and has a clear separation between input and output, which avoids the undesirable circularity discussed above.

At present, it remains unexplored the degree to which MLR-SIF is scalable across biomes and environmental conditions, and whether it has any practical advantages for photosynthesis estimation relative to existing approaches, e.g., the conventional FvCB or a simple linear scaling from SIF reported by previous studies (Sun et al., 2017; Li et al., 2018). Mechanistically, the MLR-SIF model and the FvCB model are equivalent, given that the light and carbon reactions are balanced (Blankenship, 2002). However, these two models differ in the number and complexity of parameters required (See Notes S1 in Gu et al., 2019). The FvCB model minimally represents the light reactions via an empirical electron transport equation to focus on the mechanistic representation of the carbon reactions. No light reaction mechanisms (e.g., light harvesting, photochemical and non-photochemical quenching) are represented. The carbon reactions belong to the downstream processes in photosynthesis and are highly complex. As a result, a large number of biochemical and kinetic parameters are needed to run the FvCB model and these parameters can be highly variable across biomes and environments. Consequently, different TBMs that employ the same FvCB model show considerable disagreements in simulated photosynthesis and its response to environmental drivers; and much of the disagreements can be attributed to model parameter uncertainties (e.g., Schaefer et al., 2012; Anav et al., 2015; Rogers et al., 2017; Walker et al., 2021). The MLR-SIF model requires fewer input parameters than FvCB, because SIF<sub>PSII</sub> as an input together with  $q_L$  implicitly contains environmental and physiological information represented by the FvCB model for estimating photosynthesis (Gu et al., 2019). We thus predict that the parsimony of the MLR-SIF model can reduce the impact of parameter uncertainties for photosynthesis estimation when the extra independent information (both environmental and physiological) contained in SIF is available.

125

126

127

128

129

130

131

132

133

134

135

136

137

138

139

140

141

142

143

144

145

146

147

148

149

150

151

152

153

154

155

This study has two objectives. The first objective is to demonstrate and validate the effectiveness of the mechanistic MLR-SIF model that uses  $SIF_{PSII}$  as an input to compute photosynthesis. The second objective is to demonstrate the practical advantages of the parameter parsimoniousness of the MLR-SIF approach when facing parameter uncertainties, *i.e.*, to test the above hypothesis across a broad range of Plant Functional Types (PFTs) and dynamic environments. To our knowledge, this is the first study to demonstrate the possibility and advantage of mechanistically estimating photosynthesis from the perspective of light reactions using  $SIF_{PSII}$  as an input across a wide range of PFTs and climates. We focus on the leaf level so that fundamental processes can be more fully investigated. To achieve our objectives, we collected

concurrent measurements of leaf gas exchange and pulse amplitude modulated (PAM) ChlF for 29 species of 11 representative PFTs native to Temperate, Boreal, and Tropical climates (Table S1). Using this dataset, we unraveled the regulation of environmental and physiological variations on the dynamic relationship between  $SIF_{PSII}$  and photosynthesis across PFTs, and assessed the advantages of MLR-SIF for estimating photosynthesis in terms of the capability, scalability, and uncertainty across PFTs and environments. We demonstrate that the key value of SIF lies in the process information it contains, which reduces the number of hard-to-measure parameters and the associated uncertainties for estimating photosynthesis. Our findings should pave the way for future investigations to apply SIF as an observational input to mechanistically estimate photosynthesis at the canopy scale and beyond.

### **Materials and Methods**

#### **Derivation of the MLR-SIF model**

SIF<sub>PSII</sub> is emitted during the photosynthetic light reactions, and can be used to directly quantify the actual electron transport rate ( $J_a$ ) balanced by carboxylation and photorespiration in the carbon reactions (Blankenship, 2002), following the principle of energy conservation (Gu *et al.*, 2019). Once  $J_a$  is determined, net photosynthesis ( $A_n$ ) can be calculated based on the electron requirements of carboxylation and oxygenation (Farquhar *et al.*, 1980; Sharkey, 1985; von Caemmerer, 2000):

175 
$$A_n = A_g - R_d = \begin{cases} \frac{C_i - \Gamma^*}{4C_i + 8\Gamma^*} J_a - R_d, & \text{for C}_3 \text{ species} \\ \frac{1 - x}{3} J_a - R_d, & \text{for C}_4 \text{ species} \end{cases}$$
 Eq. 1a

$$J_a = \frac{\Phi_{PSIImax} \times (1 + k_{DF})}{1 - \Phi_{PSIImax}} \times q_L \times SIF_{PSII}$$
 Eq. 1c

Here  $A_g$  refers to gross photosynthesis;  $SIF_{PSII}$  represents the true total ChIF emitted from PSII, which in principle should be utilized to establish the mechanistic relationship with photosynthesis;  $C_i$  the intercellular  $CO_2$  concentration;  $\Gamma^*$  the  $CO_2$  compensation point in the absence of mitochondrial respiration in the light for  $C_3$  plants; x the fraction of total electron transport of mesophyll and bundle sheath allocated to the  $CO_2$ -concentrating mechanism for  $C_4$  plants;  $R_d$  the day respiration;  $\Phi_{PSIImax}$  the maximum photochemical quantum efficiency of PSII in dark-adapted leaves;  $k_{DF} = k_D/k_F$ , with  $k_D$  and  $k_F$  representing the rate constants of constitutive thermal dissipation and fluorescence, respectively;  $q_L$  is derived under the assumption of lake model for photosynthetic unit connectivity. Note that MLR-SIF applies to all carboxylation limitation states, regardless of whether the carboxylation is limited by Ribulose 1,5-bisphosphate (RuBP) regeneration, RuBP carboxylase/oxygenase (Rubisco), or triose phosphate use (TPU), because it directly models the "actual" electron transport rate  $J_a$  from  $SIF_{PSII}$  (as opposed to the "potential" electron transport rate employed in FvCB) (Gu *et al.*, 2019). As in most applications of the FvCB model, Eq. 1a assumes that the supply of NADPH, rather than ATP, from the light reactions limits carboxylation.

 $J_a$  can also be derived alternatively from  $SIF_{PSII}$  via NPQ (Gu et al., 2019):

192 
$$J_a = PAR \times \alpha \times \beta - (1 + NPQ) \times (1 + k_{DF}) \times SIF_{PSII}$$
 Eq. 2

where  $\alpha$  is leaf absorptance;  $\beta$  the fraction of absorbed light allocated to PSII.

191

193

194

195

196

197

198

199

200

201

202

203

204

205

206

207

208

209

210

211

212

213

Eq. 2 and Eq. 1c are theoretically equivalent (Gu et al., 2019), but practically have different complexity and thus applicability. Eq. 2 shows more clearly the principle of energy conservation among different dissipation pathways of absorbed photons. For actual applications, it requires PAR, NPQ, and  $SIF_{PSII}$  as inputs. Eq. 1c requires only  $SIF_{PSII}$  and  $q_L$ .  $q_L$  reflects the redox state of PSII and provides a good steady-state approximation of the state of Cytochrome b6f (Cyt b6f) which plays a central role in the control of steady-state photosynthesis (Johnson & Berry, 2021). NPQ involves both energetic and enzymatic reactions. Although the heat dissipation from NPQ is predominantly localized in the light-harvesting complexes of PSII, the activation and regulations of this release occur in the lumen, thylakoid membrane, and stroma. NPQ has a delayed response to light variations (Kromdijk et al., 2016), a property that is exploited in PAM fluorometry to transiently decouple the photochemical and non-photochemical quenching to calculate various fluorescence variables (e.g.,  $\Phi_P$ , NPQ, and  $q_L$ ). Furthermore, NPQ has multiple components (e.g., the energy-dependent qE, the irreversible components qI and qZ, and state transitions qT) and each operates at different time scales (Ruban, 2016, Nilkens et al., 2010, Demmig-Adams et al., 2014). The complex activation and regulations, delayed time response, and involvement of multiple time scales in the dynamics of NPO components greatly increase the complexity in modeling NPO as compared to  $q_L$ . Thus, we choose the  $q_L$ -based approach for calculating  $J_a$  from  $SIF_{PSII}$  which simplifies the mechanistic modeling of photosynthesis as advocated in Gu et al. (2019). As PAM only measures ChlF parameters but not SIF<sub>PSII</sub> itself, we had to derive SIF<sub>PSII</sub> from the following theoretical equations (Gu et al., 2019):

$$SIF_{PSII} = \Phi_F \times PAR \times \alpha \times \beta$$
 Eq. 3

215 
$$\Phi_F = \frac{1 - \Phi_{PSIImax}}{(1 + k_{DF}) \times [(1 + NPQ) \times (1 - \Phi_{PSIImax}) + q_L \times \Phi_{PSIImax}]}$$
 Eq. 4

Here, we used  $\Phi_{PSIImax}$ , NPQ and  $q_L$  inferred from PAM measurements to derive  $SIF_{PSII}$  (full list of symbols/variables defined in Table S2). Note that if  $SIF_{PSII}$  is available as an observational input

(*i.e.*, inferred from direct observables), we do not need to model  $SIF_{PSII}$ , but simply use Eq. 1c (in this case, NPQ is not needed) to compute  $J_a$  and therefore photosynthesis. Even though it is indeed now possible to measure leaf-level ChIF emission spectra (in absolute radiometric units, *e.g.*, Magney *et al.*, 2019b; Meeker *et al.*, 2021), such measurements always contain contributions from PSII and PSI, while in theory  $SIF_{PSII}$  is required to estimate photosynthesis (Eq. 1). Also, such measurements cannot resolve the issue of leaf re-absorption of fluorescence. Together these factors mean that direct fluorescence emission measurements in the absolute radiometric units unavoidably contain uncertainties. Furthermore, spectral fluorescence measurements have yet to be widely collected for diverse biomes under dynamic natural environments, as utilized in this study. Balancing consideration of these factors, we first used direct leaf-level ChIF emission spectra measurements as a qualitative check for the realism of the theoretically-derived  $SIF_{PSII}$  (see supporting information in Notes S1 and Fig. S1 for the validation of  $SIF_{PSII}$ ). Subsequently, the theoretically-derived  $SIF_{PSII}$  (Eq. 3) was used to estimate photosynthesis (Eq. 1) across all plant species in our main analyses.

Note that  $SIF_{PSII}$  (Eq. 3) is the physiologically determined, spectrally and hemispherically integrated fluorescence emission in quantum unit, whereas in the remote sensing community, SIF is often given as radiance at a specific wavelength given in power unit per solid angle. From the point of view of probing photosynthesis, only the physiologically determined, spectrally and hemispherically integrated fluorescence emission in quantum unit is meaningful.

In this study, the parameters  $\alpha$  and  $\beta$  are assumed constant at 0.84 (Björkman & Demmig, 1987, Schreiber, 2004) and 0.5 (von Caemmerer, 2000), respectively. Gu *et al.* (2019) set  $k_{DF}$  to 19 using the normalized values of  $k_D$  and  $k_F$  used in van der Tol *et al.* (2014). This study utilized a  $k_{DF}$  value of 10, as inferred from Pfündel (1998). This value was further corroborated by Tesa *et al.* (2018) with actual measurements (see their Fig. 6).

### Plant species and their growth environment

We collected concurrent measurements of leaf gas exchange and ChlF parameters using PAM fluorometry for 29 species (25  $C_3$  and 4  $C_4$ ) that are representative of major PFTs (commonly adopted by TBMs) across the globe (Table S1). Measurements were taken at four locations:

Cornell Botanic Gardens (CBG), Cornell Musgrave Research Farm (CMRF), Oak Ridge National
Lab (ORNL), and Xishuangbanna Tropical Botanical Garden (XTBG) (Table S1). The
meteorological data and other growth environmental information at these four locations were
described in Notes S2. This dataset was utilized to demonstrate the possibility and advantage in
mechanistically estimating photosynthesis from the perspective of light reactions using *SIF*<sub>PSII</sub> as
an input (Eq. 1) across a wide range of PFTs and climates at the leaf scale.

## Measurements of concurrent leaf gas exchanges and ChlF parameters with PAM

- Nineteen among all the 29 species were measured with both light and CO<sub>2</sub> response curves, while 253 254 only light response curves were collected for the remaining species (Table S1). For each light or CO<sub>2</sub> response curve, we selected 3-4 healthy and fully expanded sunlit leaves as replicates of each 255 species. The specific procedures for measuring light and CO2 response curves are described in 256 Notes S3. Gas-exchange variables ( $A_n$  and  $C_i$ ), steady-state and maximum ChlF under light ( $F_s$  and 257  $F_{\rm m}$ ') were obtained from light and CO<sub>2</sub> response curves. After sequentially collecting light and 258 CO<sub>2</sub> response curves for the same leaves, we subsequently measured the maximum and minimum 259 ChlF under fully dark-adapted conditions ( $F_{\rm m}$  and  $F_{\rm o}$ ) for each leaf replicate (see procedure in 260 Notes S3). These measured ChIF parameters were in turn used to calculate  $\Phi_{PSIImax}$ 261  $(\Phi_{PSIImax} = \frac{F_m - F_o}{F_m})$ , the minimum ChlF under light  $(F_o' = \frac{F_o}{\Phi_{PSIImax} + \frac{F_o}{F_{m}'}})$ , Oxborough & Baker, 1997), 262
- 263  $q_L (q_L = \frac{F'_m F_s}{F'_m F'_o} \times \frac{F'_o}{F_s})$ , NPQ (NPQ= $\frac{F_m F'_m}{F'_m}$ ),  $\Phi_F$  (Eq. 4), and  $SIF_{PSII}$  (Eq. 3).

#### Data processing and analysis

252

264

Parameter fitting and aggregation: The MLR-SIF model (Eq. 1) requires the following parameters and driving variables as input: four parameters ( $\Phi_{PSIImax}$ ,  $k_{DF}$ ,  $\Gamma^*$ ,  $R_d$ ) and three variables ( $C_i$ ,  $q_L$ , and  $SIF_{PSII}$ ) for  $C_3$ , four parameters ( $\Phi_{PSIImax}$ ,  $k_{DF}$ , x,  $R_d$ ) and two variables ( $q_L$  and  $SIF_{PSII}$ ) for  $C_4$ . At the leaf level, these variables and  $\Phi_{PSIImax}$  can either be directly measured (e.g.,  $C_i$ ) or inferred from measurements (e.g.,  $SIF_{PSII}$ ,  $\Phi_{PSIImax}$  and  $q_L$ ), and thus can be readily incorporated into Eq. 1. Specifically, the set of parameters ( $\Gamma^*$ ,  $R_d$ , x) were derived by fitting the MLR-SIF model with data that met the quality control criteria (see Notes S4) using

scipy.optimize.curve\_fit script in Spyder 3.8. This fitting procedure was performed separately for each leaf replicate of all species.

We designed a parsimonious function to explicitly model  $q_L$  as a function of PAR instead of treating it as an input variable. The rationale here is that, although SIF observations can be readily available from remotely sensed measurements,  $q_L$  is usually not available at regional/global scale. We used an exponential equation with two parameters  $(a_{q_L}$  and  $b_{q_L})$  to represent the relationship between  $q_L$  and PAR, a parsimonious formulation that can take advantage of available PAR:

$$q_L = a_{q_L} e^{-b_{q_L} PAR}$$
 Eq. 5

Here  $a_{q_L}$  and  $b_{q_L}$  were derived by fitting this exponential equation with  $q_L$  inferred from ChIF and PAR measured by Li-6800 and/or GFS3000 for each leaf of all species. The means of the fitted  $a_{q_L}$  and  $b_{q_L}$  were then calculated across all leaves for each PFT, which were used to calculate  $q_L$  for each leaf in the corresponding PFT. The fitted and observed  $q_L$  agree well with each other for different PFTs (Fig. S2). Although this parsimonious model does not account for the impact of variation in  $C_i$  on  $q_L$ , it is adequate to capture the first-order variations in  $q_L$  in natural conditions. This is because that  $C_i$  covaries with PAR in order to keep the balance between light and carbon reactions of photosynthesis, thus the parsimonious  $q_L$  model as function of PAR is not independent of the changes in  $C_i$ . Moreover, if we deliberately force the model to "fail" in experiments by holding PAR at a high constant value and changing  $C_i$ , there would be two scenarios: 1)  $q_L$  would vary with  $C_i$  but only within a narrow range, unless  $C_i$  is made close to zero; 2) when  $C_i$  is close to zero,  $q_L$  will have to be close to zero too because the Calvin-Benson cycle cannot support any electron transport. Neither of these scenarios occurs in nature.

For MLR-SIF, once its parameters were fitted ( $\Gamma^*$ ,  $R_d$ , x,  $a_{q_L}$  and  $b_{q_L}$ ) or derived ( $\Phi_{PSIImax}$ ) for each leaf replicate under 25 °C, we obtained "PFT-specific" parameter values by averaging fitted parameters across all species within the same PFT, and "PFT-universal" parameter values by averaging fitted parameters across all species of all PFTs respectively (Table S3). Details of parameter fitting and aggregation to PFT levels can be found in Fig. S3. Note that the motivation of PFT-level parameter aggregation is to avoid the needs for acquiring plant traits for individual

species which are challenging to obtain for global applications, the eventual goal of the MLR-SIF application. On the other hand, considering only 29 plant species were employed in this study and in some cases a PFT is characterized by only one or two species, we reported our statistical assessment (in Results) using datasets from all plant species instead of that aggregated to PFT.

300

301

302

303

304

305

306

307

308

309

310

311

312

313

314

315

316

317

318

319

320

321

322

323

324

325

326

327

328

To enable comparison with the conventional FvCB model, we further derived key relevant parameters required by FvCB (including the maximum carboxylation rate-V<sub>cmax</sub>, maximum electron transport rate- $J_{\text{max}}$ ,  $\Gamma^*$ , and  $R_{\text{d}}$ ) through parameter fitting utilizing measured CO<sub>2</sub> response curves in conjunction with the corresponding light response curves (see Notes S5 for detailed procedures) for the same leaf replicate across all species of a subset of six  $C_3$  PFTs. These six PFTs used here are BDT-Temperate, BDS-Temperate, BDT-Boreal, NET-Boreal, C<sub>3</sub> Crop and C<sub>3</sub> grass. For a fair comparison of the performance between MLR-SIF and FvCB models in estimating photosynthesis, only the six  $C_3$  PFTs with both CO<sub>2</sub> and light response curves available were used to obtain "PFT-specific" and "PFT-universal" parameters for both models. The parameters required by FvCB are  $\Phi_{PSIImax}$ ,  $\Gamma^*$ ,  $R_d$ ,  $V_{cmax}$ ,  $J_{max}$ , the fraction of absorbed light allocated to PSII  $\beta$ , the curvature parameter  $\theta$ , and the Michaelis-Menten coefficients of Rubisco –  $K_{co}$ , where  $K_{\rm co} = K_{\rm c} (1 + {\rm O}/K_{\rm o})$ .  $\Phi_{\rm PSIImax}$  was inferred from PAM.  $K_{\rm c}$ ,  $K_{\rm o}$ ,  $\theta$ , and  $\beta$  were assumed as constants. Specifically, we adopted in vivo values for  $K_c$  (i.e., 404.9  $\mu$ mol mol<sup>-1</sup>) and  $K_o$  (i.e., 278.4  $\mu$ mol mol<sup>-1</sup> <sup>1</sup>) provided by Bernacchi et al., (2001);  $\theta$  was assumed to be 0.9 (Medlyn et al., 2002) and  $\beta$ assumed to be 0.5 (von Caemmerer, 2000). The remaining parameters, i.e.,  $V_{\rm cmax}$ ,  $J_{\rm max}$ ,  $\Gamma^*$ , and  $R_{\rm d}$ , were fitted by using the python optimization Scipy in Spyder 3.8. Note that we decided to fit only the four parameters here but pre-set others (to standard literature values), due to the consideration of balancing the degree of freedom (that represents the most variability in  $A_n$ ) and the goodness of model-data fitting.

Validation of the MLR-SIF model: We first assessed the fitted parameters using the leaveone-out cross-validation for each species. Specifically, MLR-SIF is trained on all samples except for one replicate and a validation is made for that replicate, and we repeat this process N times for each species (N = the replicate number of each species). The parameters under assessment included  $a_{q_L}$ ,  $b_{q_L}$ ,  $\Phi_{PSIImax}$ ,  $\Gamma^*$  (for  $C_3$ ), x (for  $C_4$ ), and  $R_d$ . Fig. S4 shows that the RMSE between the modeled  $A_n$  computed with parameters obtained from the training group and the actual observed  $A_{\rm n}$  is 2.42 µmol m<sup>-2</sup> s<sup>-1</sup> for the validation group, suggesting that the parameters fitted from the training group well captures that of the validation group.

Next, we refitted the parameters for each leaf replicate for demonstrating the performance of the MLR-SIF model across PFTs, light levels, and temperatures. Here the PFT-specific parameters ( $a_{q_L}$ ,  $b_{q_L}$ ,  $R_d$ ,  $\Gamma^*$ , x, and  $\Phi_{PSIImax}$ ) were used to estimate photosynthesis by combining measured  $C_i$  and  $SIF_{PSII}$  of each leaf replicate in the corresponding PFT (Fig. S3). We further validated the robustness of the MLR-SIF under different temperatures (20, 25, 30, 35, 40 °C) using a subset of species (for which measurements under different temperatures were made) for illustrative purpose, including  $C_3$  ( $Cornus\ racemosa\ 'Cuyzam'$ ) and  $C_4$  ( $Andropogon\ gerardii$ ). This test is similar to the above demonstration of MLR-SIF performance across PFTs, except that the averages of the parameters of all the replicates within the same species at the reference temperature (25 °C), rather than PFT-specific parameters were used to estimate photosynthesis of each leaf replicate under different temperatures.

Assessment of parameter sensitivity and the propagated estimation uncertainty (PEU) in estimated  $A_n$ : We performed two independent analyses to assess the parameter sensitivity of MLR-SIF and PEU in  $A_n$  resulted from model parameter uncertainties. In the first analysis, we utilized the PFT-universal parameters to estimate photosynthesis of each leaf replicate. To examine which input parameter the MLR-SIF model is most sensitive to, we altered each parameter one at a time to be the corresponding PFT-universal value while keeping the remaining parameter values to be PFT-specific. Parameters examined here are:  $\Gamma^*$  ( $C_3$  only), x ( $C_4$  only), as well as those shared by  $C_3$  and  $C_4$ , including  $\Phi_{PSIImax}$ ,  $R_d$ ,  $a_{q_1}$  and  $b_{q_2}$ .

In the second analysis, we assessed the uncertainty on the estimated  $A_n$  propagated from model parameter uncertainties utilizing Monte Carlo simulations for both MLR-SIF and FvCB models under different light levels (100, 300, 500, 800, 1000, and 1200  $\mu$ mol photon m<sup>-2</sup> s<sup>-1</sup>) at CO<sub>2</sub> concentration of 400  $\mu$ mol CO<sub>2</sub> mol<sup>-1</sup> and 25 °C. The uncertainty assessment here was exemplified by a single PFT, *i.e.*, BDT Temperate, for illustrative purposes. Specifically, for each model, we perturbed its parameters by randomly drawing values from their corresponding parameter distribution. For each parameter, we assumed that their values follow a Gaussian distribution, with the fitted values and the standard errors directly returned by the Scipy

optimization package for each individual leaf replicate. Here, we focus on perturbing parameters that were fitted (most influential), *i.e.*,  $a_{q_L}$ ,  $b_{q_L}$ ,  $\Gamma^*$ , and  $R_{\rm d}$  for MLR-SIF,  $V_{\rm cmax}$ ,  $J_{\rm max}$ ,  $\Gamma^*$ , and  $R_{\rm d}$  for FvCB. For each model, we randomly drew 50,000 combinations of these parameters, calculated the corresponding  $A_{\rm n}$ , and derived the standard deviation (SD) of the resulting  $A_{\rm n}$ , which is denoted as the PEU. Note that, the randomly drawn 50,000  $V_{\rm cmax}$  and  $J_{\rm max}$  were highly linearly correlated (Wullschleger, 1993; Walker *et al.*, 2014). Also, we constrained the randomly generated parameters to their physically meaningful ranges, *i.e.*  $0 < a_{q_L} < 1$ ,  $b_{q_L} < 0$ , and  $V_{\rm cmax}$ ,  $J_{\rm max}$ ,  $\Gamma^*$ , and  $R_{\rm d}$  were all positive.

#### Results

367

368

369

370

371

372

373

374

375

376

377

378

379

380

381

382

383

384

385

386

388

389

390

## The dynamic relationship between photosynthesis and SIF<sub>PSII</sub>

We first employed direct leaf-level ChlF emission spectra measurements (SIF<sub>abaxial</sub>) to verify the realism of the modeled theoretical SIF<sub>PSII</sub> (Notes S1). Our results (Fig. S1) show that SIF<sub>PSII</sub> is highly correlated with  $SIF_{abaxial}$  with  $R^2$  ranging from 0.75 to 0.95 for three crop species (almond, grape, and walnut) under well-watered, mild, and moderate drought conditions (Table S4). With confidence gained in cross-checking the theoretically modeled SIF<sub>PSII</sub> with measured SIF<sub>abaxial</sub>, we subsequently evaluated the relationships between measured  $A_n$  and theoretical  $SIF_{PSII}$  for all plant species (Table S1) that cover a much broader PFTs and environments. We found a nonlinear relationship between  $A_n$  and  $SIF_{PSII}$  across all  $C_3$  and  $C_4$  plant species (Fig. 1a; Fig. S5) and temperatures (Fig. 1b-c). This relationship is characterized by an initial increase of  $A_n$  and then leveling-off when SIF<sub>PSII</sub> is high, because the former saturates while the latter can keep increasing under high light as predicted by Gu et al. (2019). However, the saturation level of  $A_n$  and the rate approaching saturation differ considerably among species (especially between  $C_3$  and  $C_4$  plants) and temperatures. For instance, C<sub>4</sub> plants overall exhibit a higher light saturation level and slower rate towards saturation than  $C_3$  plants, resulting in a lower degree of nonlinearity for the former, consistent with patterns observed at the canopy scale (e.g., Liu et al., 2017; He et al., 2020). Notably, different species within the same PFT also show disparate  $A_n$ -SIF<sub>PSII</sub> relationships (Fig. S5). Temperatures further impact the degree of  $A_n$ -SIF<sub>PSII</sub> nonlinearity even for the same species and have distinct influences for  $C_3$  and  $C_4$  plants (Fig. 1b,c).

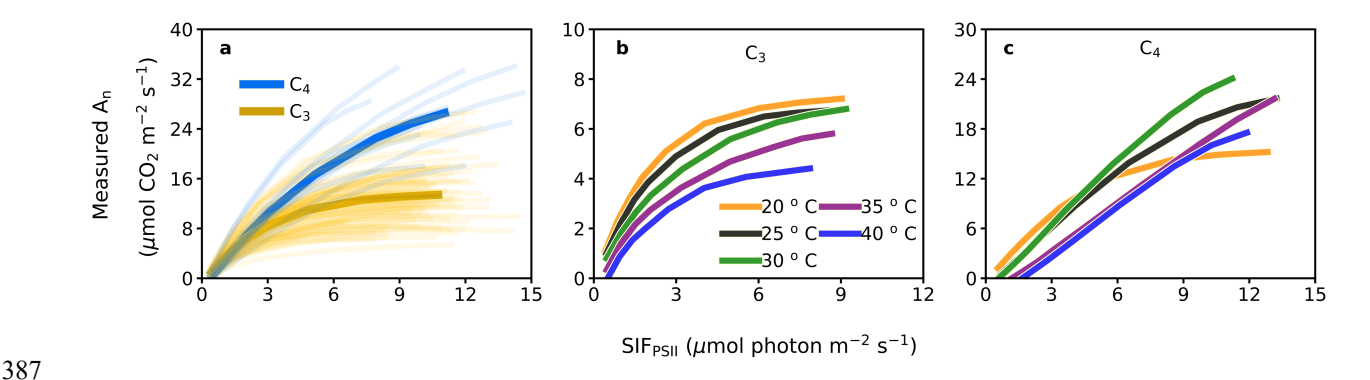


Fig. 1. The dynamic relationships between net photosynthesis  $(A_n)$  and chlorophyll a fluorescence from PSII  $(SIF_{PSII})$  across Plant Functional Types (PFTs) and environments. (a) the  $A_n$ -SIF<sub>PSII</sub> relationships across all  $C_3$  and  $C_4$  species; the thin and bold curves represent

individual leaf replicates and the mean of all species under the same photosynthetic pathways, respectively; (**b and c**) the impact of temperatures on the  $A_n$ -SIF<sub>PSII</sub> relationship for a subset of species for  $C_3$  (Cornus racemosa 'Cuyzam') and  $C_4$  (Andropogon gerardii) respectively; curves represent the mean of leaf replicates under the same temperatures.

We found relatively higher inter-species variability in NPQ than in  $q_L$  (Fig. S6), resulting in more complex relationships among NPQ,  $SIF_{PSII}$  and  $A_n$  (Fig. 2a, b). Temperature had greater impact on NPQ than on  $q_L$  (Fig. 2c, d). Across light levels, NPQ achieves a local minimum at the optimal temperature for photosynthesis (Fig. 2d). In contrast, PAR dominates the variation of  $q_L$ , with temperature playing a minor role, supporting the use of PAR as a primary predictor to capture the first order variation in  $q_L$  (Fig. 2c).

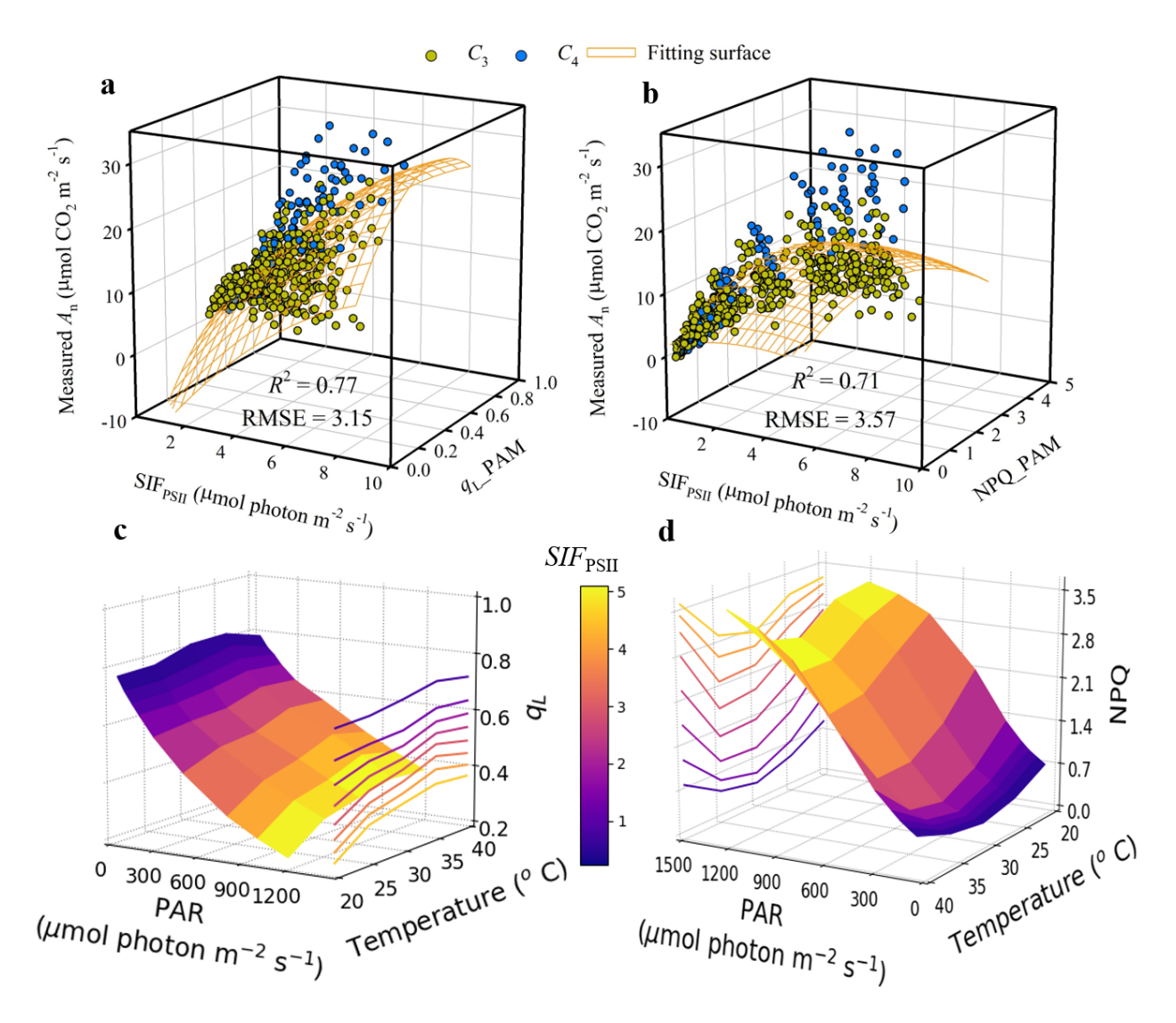


Fig. 2. The dynamic net photosynthesis  $(A_n)$  - chlorophyll a fluorescence from PSII  $(SIF_{PSII})$  relationships modulated by the fraction of open PSII reaction centers  $(q_L)$  and non-photochemical quenching (NPQ) across Plant Functional Types (PFTs) and environments. (a and b) the relationships among  $q_L$ , NPQ,  $A_n$ , and  $SIF_{PSII}$  in 3D space across all species, the corresponding 2D figures are shown in Fig. S7; statistics ( $R^2$  and RMSE) were obtained by fitting the 3D data with polynomial regression. (c and d) the impact of PAR and temperatures on  $q_L$  and NPQ, using a single  $C_3$  species ( $Cornus\ racemosa\ 'Cuyzam'$ ) for illustrative purposes.

### The capability, scalability, and uncertainty of MLR-SIF in estimating photosynthesis

The MLR-SIF model requires knowledge of  $q_L$  and  $C_i$ , which are dynamic. Using a minimalistic approach, we modeled  $q_L$  as a decreasing function of PAR with only two parameters  $a_{q_I}$  and

 $b_{q_L}$  (Eq. 5), since PAR captures the first-order effect in  $q_L$  variations (Fig. 2c, Fig. S6a). This parsimonious  $q_L$  model works reasonably well for a wide range of species (Fig. S2), which enables examining the potential of applying MLR-SIF across climates and biomes, a necessary step towards global applications.

With the use of PFT-specific parameter values, a common practice in TBMs, MLR-SIF successfully reproduces the variation of measured  $A_n$  with changing light ( $R^2 = 0.83$ , regression slope = 0.92) across all major PFTs (Fig. 3a). Moreover, MLR-SIF is capable of simulating  $A_n$  dynamics under different temperatures for both  $C_3$  and  $C_4$  (Fig. 3c-d), even though parameters were obtained solely at the reference temperature.

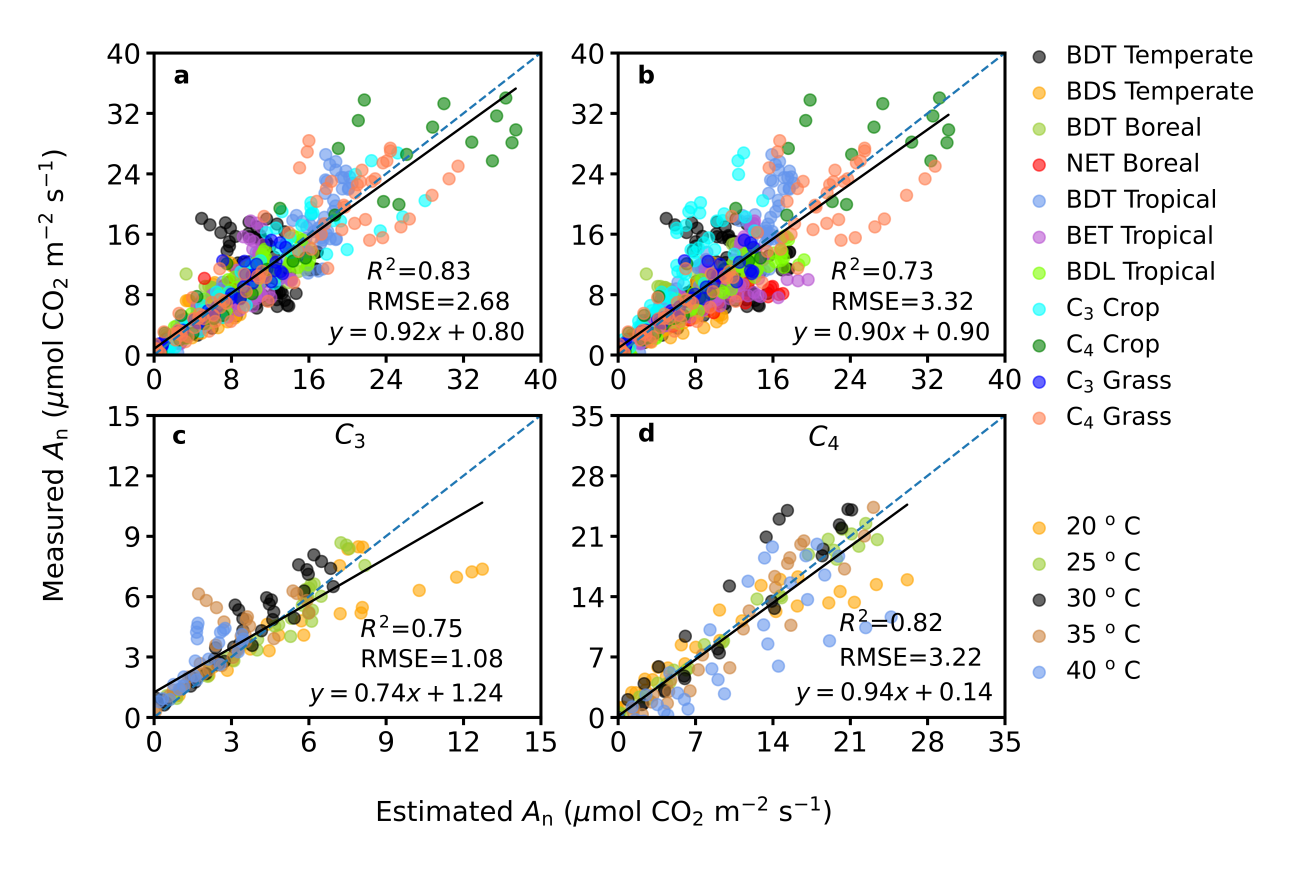


Fig. 3. Assessment of the estimated net photosynthesis  $(A_n)$  based on MLR-SIF (*i.e.*, mechanistic light reaction model with chlorophyll a fluorescence from PSII as an input, Eq. 1) against measurements across (a and b) Plant Functional Types (PFTs) and (c and d) temperatures. (a and b) estimated  $A_n$  using PFT-specific and PFT-universal parameters (Table S3) respectively under variable light conditions at 25 °C for all species (Table S1); parameters required are:  $\Gamma^*$  ( $C_3$  only), x ( $C_4$  only), and  $\Phi_{PSIImax}$ ,  $R_d$ , as well as  $a_{q_L}$  and  $b_{q_L}$  for calculating  $q_L$ 

(shared by  $C_3$  and  $C_4$ ); (**c and d**) estimated  $A_n$  under five temperatures for  $C_3$  (Cornus racemosa 'Cuyzam') and  $C_4$  (Andropogon gerardii) respectively.  $\Gamma^*$  and  $R_d$  are adjusted with a temperature response function (Bernacchi et al., 2002); remaining parameters were set to values at 25 °C. Colored scatters represent individual leaf replicates (**a and b**, color-coded by different PFTs; **c and d**, color-coded by different temperatures). The regression coefficients ( $R^2$ , RMSE, regression slope and intercept) were obtained by combining all species across PFTs (**a-b**) and temperatures (**c-d**). Solid lines represent the ordinary least square regression of all colored points; the dashed line represents 1:1.

To further demonstrate the advantages of MLR-SIF, we performed two independent analyses. First, we removed the PFT-specific parameters in MLR-SIF and evaluated how much the estimated  $A_n$  degrades if a constant value is used across all PFTs for each parameter. We found that, if using PFT-universal parameters (refer to Fig. S3 for details), the estimated  $A_n$  could still explain 73% of the variation in the measured  $A_n$  under changing light, and the estimation bias was minimal with a regression slope of 0.90 (Fig. 3b). The loss of explanation power (relative to PFTspecific values) comes from the combination of parameters uncertainty (Fig. S8a), i.e.,  $a_{q_L}$ ,  $b_{q_L}$ ,  $\Gamma^*$  (C<sub>3</sub>) or x (C<sub>4</sub>),  $R_d$  and  $\Phi_{PSIImax}$ . In addition, we used the same PFT dataset to compare the performance of MLR-SIF and FvCB models. FvCB had an overall weaker capability in estimating photosynthesis than MLR-SIF for both PFT-specific and PFT-universal parameters (Fig. 4a-d). Specifically, relative to MLR-SIF, FvCB showed a larger bias (underestimation) with a regression slope of 0.80 as compared to 0.86 for MLR-SIF for PFT-specific (Fig. 4a-b), 0.71 vs 0.81 for PFTuniversal (Fig. 4c-d), albeit both models exhibited similar  $R^2$  and RMSE. This performance difference is not due to difference in models' theoretical rigor (both MLR-SIF and FvCB are mechanistically equivalent) but due to differences in the level of parameter requirements and the associated impacts of the parameter uncertainties in model applications. All the differences between MLR-SIF and FvCB shown below should be interpreted this way.

In the second analysis, we used Monte Carlo simulations to explicitly quantify the uncertainty in  $A_n$  propagated from model parameter errors. We compared PEU between MLR-SIF and FvCB using Temperate Broadleaf Deciduous Tree (BDT Temperate) as an example (Fig. 4e, f). Our results showed that MLR-SIF consistently exhibits lower PEU than FvCB under all light

conditions (Fig. 4e). Correspondingly,  $A_n$  estimated with MLR-SIF tends to have a narrower statistical distribution relative to FvCB (Fig. 4f).

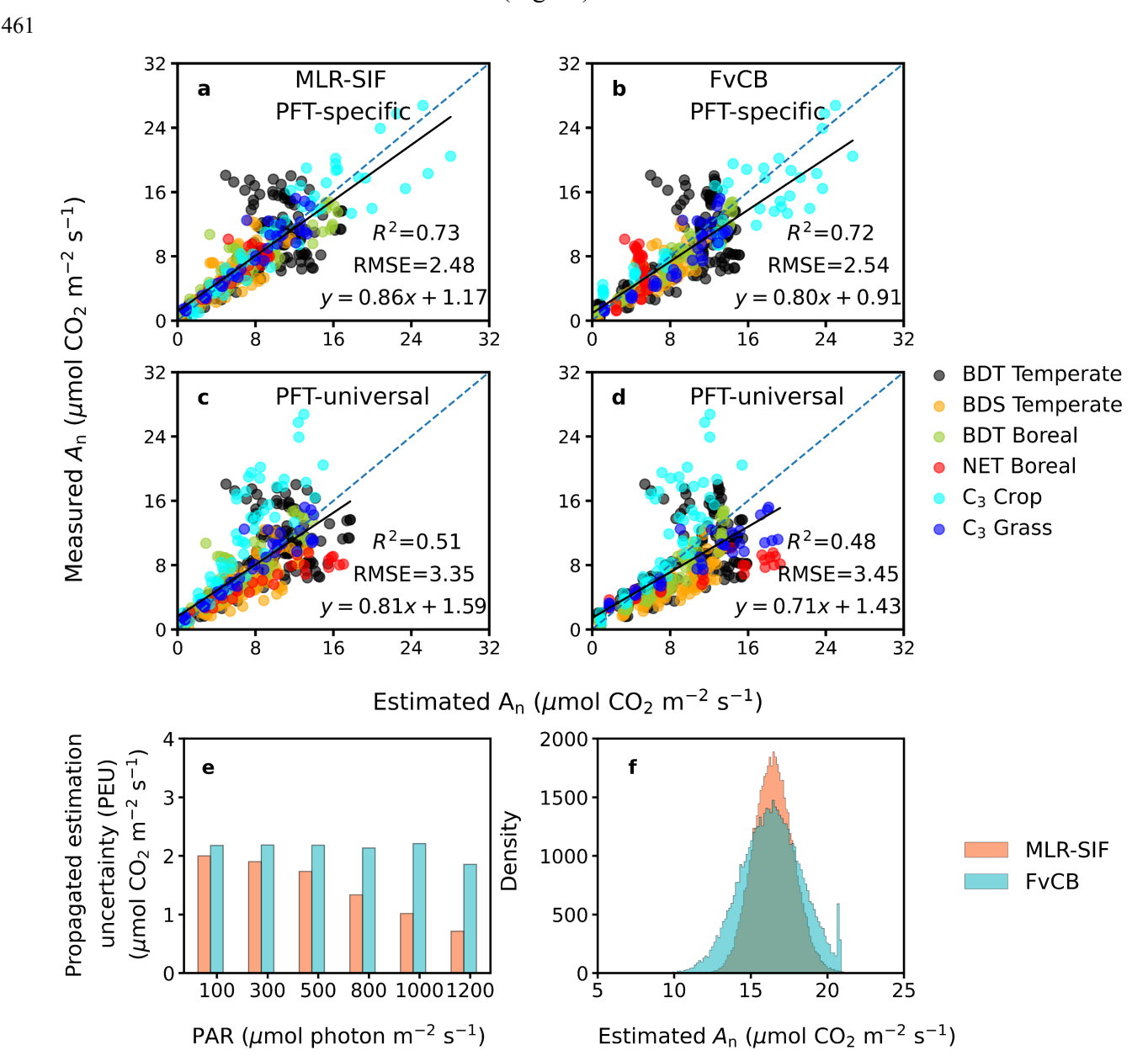


Fig. 4. Comparison of MLR-SIF (*i.e.*, mechanistic light reaction model with chlorophyll a fluorescence from PSII as an input) and FvCB (*i.e.*, Farquhar, von Caemmerer, Berry model) in estimating net photosynthesis ( $A_n$ ) (a to d) and the propagated estimation uncertainty (PEU) in  $A_n$  from parameter perturbation using Monte Carlo simulations (e and f). (a and c) are similar to Fig. 3 a and b, except that only six  $C_3$  Plant Functional Types (PFTs)

(for which both CO<sub>2</sub> and light response curves are available) were used, to ensure fair comparison of MLR-SIF and FvCB. (**b and d**) parameters required for FvCB are: the maximum photochemical quantum efficiency of PSII in dark-adapted leaves ( $\Phi_{PSIImax}$ ), the CO<sub>2</sub> compensation point in the absence of mitochondrial respiration in the light ( $\Gamma^*$ ), day respiration ( $R_d$ ), the maximum carboxylation rate ( $V_{cmax}$ ), and maximum electron transport rate ( $J_{max}$ ). (**a to d**) the regression coefficients ( $R^2$ , RMSE, regression slope and intercept) were obtained by combining all species of six  $C_3$  PFTs. (**e**) PEU, quantified as the standard deviation in  $A_n$  estimated with randomly perturbed parameters under different light levels. For illustration purposes, only Temperate Broadleaf Deciduous Tree (BDT Temperate) was used in this analysis. (**f**) histograms of estimated  $A_n$  for MLR-SIF and FvCB at PAR = 1200 µmol photon m<sup>-2</sup> s<sup>-1</sup>.

#### Discussion

479

480

481

482

483

484

485

486

487

488

489

490

491

492

493

494

495

496

497

498

499

500

501

502

503

504

505

506

507

508

509

# The physiological and environmental controls on the photosynthesis-SIF<sub>PSII</sub> relationship

The relationship between photosynthesis and SIF<sub>PSII</sub> across all plant species and temperatures is close to a linear correlation at low light, especially for  $C_4$  plant species. But the overall shape is non-linear (Figs. 1-2), which reveals that the variations in  $q_L$  and  $C_i$  prevent an exclusive dependence of photosynthesis on  $SIF_{PSII}$  (Eq. 1). Indeed,  $q_L$  decreases with light (Fig. S6), which in turn increases the nonlinearity between photosynthesis and SIF<sub>PSII</sub> under high PAR (Fig. 2a). In addition, the responses of photosynthesis and  $SIF_{PSII}$  to  $C_i$  were not synchronized due to dynamic NPQ. For example,  $A_n$  increased initially and then reached a stable value when  $C_i$  is high (Fig. S9), whereas  $SIF_{PSII}$  can have a slight decrease at the very low  $C_i$  (for some species) and then increased to a peak followed by a subsequent decrease or remaining constant at high C<sub>i</sub> (Fig. S10). The patterns of SIF<sub>PSII</sub> vs C<sub>i</sub> shown in Fig. S10 reflect the dynamics in the impact of competitive interactions between photochemical and non-photochemical quenching on ChlF emission. At low  $C_i$ , NPQ dominates whereas the impact of photochemical quenching is limited. As  $C_i$  increases, photochemical quenching increases while NPQ weakens. This asynchrony of the responses of  $A_n$ and  $SIF_{PSII}$  to  $C_i$ , especially under the low  $C_i$  induced by constraints of stomatal conductance, explains the apparent "decoupling" of SIF and photosynthesis (i.e., high SIF and low photosynthesis) following artificially induced stomatal closure observed in single-factor analyses (Marrs et al., 2020). Under these conditions, low  $C_i$  inhibits photosynthetic carbon assimilation, and also induces low  $q_L$  and increases NPQ to dissipate excess energy to offset the elevated photooxidative stress. As a result, low  $C_i$  contributes substantially to the dynamics and complexity of the photosynthesis-SIF<sub>PSII</sub> relationship.

In previous studies, the complex environmental and physiological regulations on the photosynthesis-SIF relationship are typically hidden in the simplified term of light use efficiencies, which prevents a consistent interpretation of photosynthesis-SIF relationship across time scales, phenological stages, biomes, and environmental variations. For example, previous studies reported linear and even approximately biome-independent scaling between SIF and photosynthesis at the canopy level (e.g., Sun et al., 2017; Li et al., 2018), because they were conducted at the seasonal scale and beyond, under which scales the co-variation of SIF and photosynthesis is dominated by the temporal variability in leaf area index (LAI, and therefore fPAR) (e.g., Yang et al., 2015; Magney et al., 2020). However, the linearity tends to break down at shorter time scales (e.g., sub-

daily, Zhang *et al.*, 2016; Damm *et al.*, 2015) as analogous to the typical light response curves in this study and/or under stress (Marrs *et al.*, 2020). In the former case, LAI remains relatively stable diurnally or within a few days, the relationship between SIF and photosynthesis can deviate from being linear due to the strong physiological regulation of variables such as  $q_L$ , and/or  $C_i$ . Further, these physiological regulations can vary among phenological stages, resulting in disparate phenology-dependent photosynthesis-SIF relationships (Yang *et al.*, 2018; Miao *et al.*, 2018, 2020). On the other hand, at sub-daily timescales, decoupling of photosynthesis and SIF could occur also due to variations in APAR and escape probability arising from canopy structure and illumination-viewing geometry (Chang *et al.*, 2021). In the latter case, *e.g.*, under cases of extreme photo-oxidative stress, it is crucial to incorporate  $q_L$  and/or  $C_i$  in order to accurately interpret the coupling/decoupling of photosynthesis-SIF relationships (as explained above).

## SIF as an optical 'shortcut' reduces uncertainty from parameters in MLR-SIF

Currently, TBMs and some remote sensing products (*e.g.*, BESS, Ryu *et al.*, 2011; PR model, Keenan *et al.*, 2016) have almost exclusively adopted the FvCB biochemical model to calculate leaf photosynthesis (Farquhar *et al.*, 1980; Sharkey, 1985; von Caemmerer, 2020), with considerably variable implementation across TBMs, resulting in largely different responses of simulated photosynthesis to environmental drivers (*i.e.*, light, temperature, CO<sub>2</sub>, VPD, and soil moisture, Rogers *et al.*, 2017). Notably, the fundamental biochemical and kinetic parameters required by FvCB constitute major sources of uncertainty in simulated photosynthesis (Bonan *et al.*, 2011, 2012). For example,  $V_{\rm cmax}$  and  $J_{\rm max}$  vary widely across PFTs, and are sensitive to leaf nitrogen contents, leaf ontology, and environmental changes (Field & Mooney, 1986; Kattge *et al.*, 2009, 2020; Detto & Xu, 2020), which in turn lead to significant model output uncertainty (Walker *et al.*, 2017; Rogers *et al.*, 2017; Bonan *et al.*, 2011).

We demonstrated the capability, scalability, and effectiveness of MLR-SIF across PFTs and environments, which stems from the fact that *SIF*<sub>PSII</sub>, once inferred from direct observations (after appropriately accounting for factors such as spectral integration and escape probability), carries information on instantaneous plant functional responses to atmospheric forcings and integrates over the dynamic physiological complexities of photosynthesis. This means that MLR-SIF can circumvent estimation uncertainty propagated from model parameter errors/deficiency. For example, unlike FvCB, MLR-SIF does not rely on highly sensitive biochemical and kinetic

parameters such as  $V_{\rm cmax}$ ,  $J_{\rm max}$ , and  $K_{\rm co}$ , or selection of limitation stage of carboxylation (Walker *et al.*, 2021). Note that FvCB has larger PEU than MLR-SIF does, not because the former has a structural weakness but because the latter takes advantage of an observable photosynthetic functional 'shortcut' (SIF) (Gu *et al.*, 2019), *i.e.*, at least in theory, SIF makes estimating photosynthesis simpler although there are still difficult aspects that need to be resolved through continuing research. MLR-SIF effectively utilizes the mechanistic information in observed SIF to estimate photosynthesis in a forward way, independent from other existing photosynthesis estimation approaches that are known to have different levels of uncertainties (Kira *et al.*, 2021; Wehr *et al.*, 2016; Keenan *et al.*, 2019). Independent estimates are essential for confidence building as photosynthesis cannot be measured directly beyond a single leaf.

A recent new photosynthesis model based on Cytochrome b6f (Johnson & Berry, 2021) also established from light reaction perspective, but there are numerous differences with MLR-SIF. First of all, the model from Johnson & Berry (2021) does not use *SIF*<sub>PSII</sub> (or SIF) as an input and focuses on PSI, rather than PSII. In contrast, MLR-SIF use SIF<sub>PSII</sub> as input, and its goal is to build a physiological foundation that can mechanistically and accurately utilize SIF<sub>PSII</sub> to directly and independently estimate photosynthesis. In addition, MLR-SIF applies to all carboxylation limited states, regardless of whether the carboxylation is limited by RuBP regeneration, Rubisco, or TPU, while the model developed by Johnson & Berry (2021) aims to establish a mechanistic light reaction model that can replace the empirical light-reactions sub-model of FvCB when photosynthetic assimilation is RuBP-regeneration limited.

## Prospects of future work for facilitating MLR-SIF applications to large scales

As the first effort for building the physiological foundation towards utilizing  $SIF_{PSII}$  to mechanistically and independently estimate photosynthesis, this study starts from and focuses on the leaf level, the same as the introduction of the original FvCB model. Building the physiological foundation and gaining confidence on MLR-SIF at the leaf level is a necessary step, as existing leaf-level simulations of  $\Phi_F$ , NPQ,  $\Phi_{PSII}$  as well as their functional relationships exhibit strong discrepancy with observations and across different TBMs (Yang *et al.*, 2021; Parazoo *et al.*, 2020). Moving forward, to fully unleash the power of MLR-SIF to infer photosynthesis at large scales that are independent from currently existing photosynthesis estimates (with well-documented uncertainties), future work in the following aspects are needed.

a) Parameterization of  $q_L$  or NPQ: In principle, modeling  $J_a$  requires either  $q_L$  or NPQ (but not both) if SIF<sub>PSII</sub> could be inferred from direct observational input (Gu et al., 2019). To facilitate large-scale applications (without the needs of PAM measured  $q_L$  or NPQ),  $q_L$  or NPQ must be modeled independently. To achieve this, the present application of MLR-SIF empirically models  $q_L$  as a function of PAR. Our results confirm that this parsimonious approach can capture the first-order effect of the SIF<sub>PSII</sub>-photosynthesis relationship, as  $q_L$  reflects the redox poise of PSII reaction centers and is far more sensitive to variations in light than to other environmental variations such as temperature or CO<sub>2</sub>. Nevertheless, other environmental factors can also influence  $q_L$ . For example, temperature can play an increasing role in regulating  $q_L$  under high PAR (Fig. 2c). This will require more controlled experiments and/or synthesis of existing measurements across biomes and environmental conditions to refine our current parsimonious parameterization of  $q_L$ . Conceivably, it may be possible to mechanistically model the dynamic responses of  $q_L$  to environmental variations based on the redox relationships between reaction centers and electron carriers along the electron transport chain. Using a mechanistic  $q_L$  model will considerably improve the applicability of the MLR-SIF model. Although this study does not pursue a NPQ route for the application of the MLR-SIF model, this alternative route also has values. For example, it will promote field research in the dynamics of NPQ, which has important implications for land surface energy balance (Raczka et al., 2019), at different time scales. It will also lead to estimates of photosynthesis that are independent from those of the  $q_L$ -based MLR-SIF model when SIF is available as a direct observable input. Empirical models of NPQ that consider the memory effect of past illumination history such as that used in Zhu et al. (2004) will have some capacity to deal with the multiplicity of NPQ at different time scales and can be used as a starting point for an NPQbased MLR-SIF. Mechanistically modeling NPQ (Zaks et al., 2012) for broad applicability will be a huge challenge but will be necessary to enabling the general use of the NPQ-based MLR-SIF model at different scales.

570

571

572

573

574

575

576

577

578

579

580

581

582

583

584

585

586

587

588

589

590

591

592

593

594

595

596

597

598

599

600

b) Dynamic calculation of  $C_i$ : This study utilized measured  $C_i$  as input to MLR-SIF, with the intention to eliminate uncertainties not specifically related to  $SIF_{PSII}$ , which is our major focus here. Similarly, FvCB in this study also utilized measured  $C_i$  as an input. This way ensures a fair comparison between them in the context of leaf-level application. Moving

toward an eventual application of MLR-SIF to large scales would necessitate coupling the MLR-SIF model with stomatal conductance and energy balance models. In order to dynamically determine  $C_i$  by closing the system of equations of MLR-SIF, stomatal conductance, Fick's law of  $CO_2$  diffusion from atmosphere to leaf interior, and energy balance are required, much like how FvCB is applied in TBMs.

- c) Parameter Φ<sub>PSIImax</sub>: We employed the measured Φ<sub>PSIImax</sub> values to MLR-SIF, which range from 0.74 to 0.81 (Table S3). The slight variability in Φ<sub>PSIImax</sub> across PFTs is likely a consequence of the different leaf ages resulted from the longtime span of our measurements and perhaps also environmental stress. Fortunately, utilizing a fixed Φ<sub>PSIImax</sub> value across plant species has only very minor impacts on our results (comparing Fig. 3a with Fig. S8d), giving us confidence that it is reasonable to apply a constant Φ<sub>PSIImax</sub> for large-scale applications.
- d) Parameter  $k_{\rm DF}$ : In MLR-SIF, estimation of  $J_{\rm a}$  requires  $k_{\rm DF}$  as a parameter input. Yet, the precise value of  $k_{\rm DF}$  and the degree to which it varies across plant species are presently unknown, as it is impossible to isolate  $k_{DF}$  with the current PAM fluorometry (Gu et al., 2019). We note that the uncertainty in the precise value of  $k_{\rm DF}$  does not affect our conclusion, as it is the product term  $(1+k_{\rm DF})\times SIF_{\rm PSII}$ , instead of  $k_{\rm DF}$  itself, matters for  $J_{\rm a}$ estimation at the leaf level. Specifically,  $SIF_{PSII}$  and  $k_{DF}$  always appear together as a product term  $(1+k_{DF})\times SIF_{PSII}$  in the  $J_a$  calculations (Eq. 1c and Eq. 2). If  $k_{DF}$  increases, the modeled  $SIF_{PSII}$  must decrease in order to keep the modeled  $J_a$  meaningful (i.e., in agreement with PAM  $J_a$  measurements). On the other hand, the precise determination of  $k_{\rm DF}$  is a critical step to scale up MLR-SIF to larger-scale applications, at which, SIF can be directly observed but not its product with  $k_{\rm DF}$ . It is possible that the value of  $k_{\rm DF}$  can be constant across species, as both  $k_{\rm F}$  and  $k_{\rm D}$  are physical properties of chlorophyll molecules whose structures (e.g., electron orbitals) are highly conserved for higher plants. This argument can be implicitly supported by the highly conservative  $\Phi_{PSIImax}$  value across plant species when they are not under stress, even though there are more processes involved in determining it than  $k_F$  or  $k_D$ . In terms of potential dependence of  $k_{DF}$  on temperature, earlier work (van der Tol et al., 2014) hypothesized that k<sub>D</sub> varies with temperature. This hypothesis will need to be verified and its physical mechanisms will

- need to be identified. In the future, the value of  $k_{\rm DF}$  can be precisely determined by measuring both adaxial and abaxial fluorescence emissions, as well as leaf absorptions. This way can lead to direct measurements of the true total SIF emission from the photosystems, which together with measured  $q_{\rm L}$  and NPQ can be used to determine  $k_{\rm DF}$  (Gu *et al.*, 2019). This additionally will require the development of a leaf-level full spectral fluorescence system that is capable of separating PSII and PSI contributions.
- e) PSI and alternative electron flow: The functional stability of PSII and PSI differs under stress (Ivanov *et al.*, 2001), which might change their relative contributions to fluorescence emission. Thus, fluorescence emission from both PSII and PSI should be considered when *SIF*<sub>PSII</sub> is inferred from at-sensor SIF for the broad application of MLR-SIF. Meanwhile, when plants are under stress, alternative electron sinks other than carboxylation oxygenation may be large. These issues may affect SIF photosynthesis relationships and should be explored in the future. An integration of the PSII-focused (*i.e.*, Gu *et al.* 2019) and PSI-focused (*i.e.*, Johnson & Berry, 2021) light reaction modeling approaches may lead to new insights in this direction.
- f) Coupling MLR-SIF with leaf and canopy radiative transfer: This study starts from and focuses on the leaf level, assuming that SIF<sub>PSII</sub> can be inferred from at-sensor SIF observations. Currently, SIF<sub>PSII</sub> is built upon PAM fluorometry (as used in this study), not a directly observable. However, in theory, SIF<sub>PSII</sub> can be derived from the directly observable at-sensor SIF, and once this is achieved, we do not need PAM anymore. In reality, from SIF<sub>PSII</sub> to at-sensor SIF, multiple radiative transfer processes within the leaf and across the canopy, i.e., re-absorption and scattering (their relative strength depends on wavelength), can largely attenuate the observed signal. Therefore, large-scale applications of MLR-SIF would require a coupling with leaf/canopy radiative transfer scheme (as commonly done in TMBs) or invoking an escape probability factor determined from other means to infer SIF<sub>PSII</sub> from at-sensor SIF, a currently key research topic in SIF remote sensing (e.g., Yang et al., 2018; Liu et al., 2019; Zeng et al., 2019).

#### **Conclusions**

Here we demonstrate the possibility and advantage in mechanistically estimating photosynthesis using *SIF*<sub>PSII</sub> as an input across a wide range of PFTs and climates. The fidelity, scalability, and lower uncertainty compared with the traditional FvCB model suggests that MLR-SIF has great

potential in applying the rapidly increasing volumes of satellite SIF monitoring to estimate global photosynthesis. This model framework has similar mechanistic rigor as the conventional FvCB model but requires fewer parameters. It enables a truly independent estimate of photosynthesis based on SIF observations. The importance of SIF lies in the fact that it is a functional signal of photosynthesis and reflects collective responses of plants to environmental variations. Therefore, the availability of SIF observations can greatly ease the efforts for modeling photosynthesis by avoiding the need to explicitly and accurately represent individual environmental/physiological controls on photosynthesis (*i.e.*, which carboxylation limitation occurs under what conditions) and by reducing parameterization burdens and associated uncertainties.

## Acknowledgments

673

686

- This study is supported by NSF Macrosystem Biology (Award 1926488). JH, CYC, JW, and OK
- and YS also acknowledge support from USDA-NIFA Hatch Fund (1014740), USDA-NIFA
- postdoctoral fellowship (2018-67012-27985), NASA MEaSures project, and the United States -
- 677 Israel Binational Agricultural Research and Development Fund, Vaadia-BARD Postdoctoral
- Fellowship Award No. (FI-576-18), respectively. YZ acknowledges support from the Maine
- Agricultural and Forest Experiment Station, and the USDA-NIFA and Agriculture Hatch Fund
- 680 (ME022021). ORNL is managed by UT-Battelle, LLC, for DOE under contract DE-AC05-
- 681 00OR22725. TSM and EWM acknowledge funding from the NASA ECOSTRESS (proposal # 18-
- 682 ECOSTRES18-0056) program. We thank Sharon Ng and Paul Stachowski for their invaluable
- 683 field assistance, Lailiang Cheng, Jed Sparks, and Shi-Jian Yang for sharing needed instruments
- and facilities, as well as Yan Xiao and Ting Wang for collecting measurements at Xishuangbanna
- 685 Tropical Botanical Garden.

#### **Author contributions**

- JH and YS planned and designed the research. JH, CY-YC, YZ, EWM, TSM, JW, OK, and SM
- 688 performed experiments. JH analyzed data. JH, LG and YS wrote the manuscript. CY-YC and APW
- edited the manuscript.

### 690 **Data Availability**

- 691 Data are available from the Cornell University eCommons Repository at
- 692 https://doi.org/10.7298/q3hb-zq56.

#### References

5

15

20

- Anav A, Friedlingstein P, Beer C, Ciais P, Harper A, Jones C, Murray-Tortarolo G, Papale D, Parazoo NC, Peylin P et al. 2015. Spatiotemporal patterns of terrestrial gross primary production: A review. *Review of Geophysics* 53: 785–818.
- Bacour C, Maignan F, MacBean N, Porcar-Castell A, Flexas J, Frankenberg C, Peylin P, Chevallier F, Vuichard N, Bastrikov V. 2019. Improving estimates of gross primary productivity by assimilating solar induced fluorescence satellite retrievals in a terrestrial biosphere model using a process based SIF model. *Journal of Geophysical Research: Biogeosciences* 124: 3281–3306.
- Beer C, Reichstein M, Tomelleri E, Ciais P, Jung M, Carvalhais N, Rödenbeck C, Arain MA, Baldocchi D, Bonan GB et al. 2010. Terrestrial gross carbon dioxide uptake: global distribution and covariation with climate. *Science* 329: 834–838.
  - Bernacchi CJ, Singsaas EL, Pimentel C, Portis AR, Long SP. 2001. Improved temperature response function for models of Rubisco-limited photosynthesis. *Plant, Cell and Environment* 24: 253–259.
  - **Bernacchi CJ, Portis AR, Nakano H, von Caemmerer S, Long SP. 2002.** Temperature response of mesophyll conductance. Implications for the determination of Rubisco enzyme kinetics and for limitations to photosynthesis in vivo. *Plant Physiology* **130:** 1992–1998.
  - **Björkman O, Demmig B. 1987.** Photon yield of O<sub>2</sub> evolution and chlorophyll fluorescence characteristics at 77 K among vascular plants of diverse origins. *Planta* **170**: 489–504.
  - Blankenship RE. 2002. Molecular Mechanisms of Photosynthesis (Blackwell Science, Oxford).
  - Bonan GB, Lawrence PJ, Oleson KW, Levis S, Jung M, Reichstein M, Lawrence DM, Swenson SC. 2011. Improving canopy processes in the Community Land Model version 4(CLM4) using global flux fields empirically inferred from FLUXNET data. *Journal of Geophysical Research* 116: G02014.
  - Bonan GB, Oleson KW, Fisher RA, Lasslop G, Reichstein M. 2012. Reconciling leaf

- physiological traits and canopy flux data: Use of the TRY and FLUXNET databases in the Community Land Model version 4. *Journal of Geophysical research* **117:** G02026.
- Chang CY, Wen J, Han J, Kira O, LeVonne J, Melkonian J, Riha SJ, Skovira J, Ng S, Gu L, Wood JD, Nathe P, Sun Y. 2021. Unpacking the drivers of diurnal dynamics of sun-induced chlorophyll fluorescence (SIF): Canopy structure, plant physiology, instrument configuration and retrieval methods. *Remote Sensing of Environment* 265: 112672.

10

- Ciais P, Dolman AJ, Bombelli A, Duren R, Peregon A, Rayner PJ, Miller C, Gobron N, Kinderman G, Marland G et al. 2014. Current systematic carbon-cycle observations and the need for implementing a policy-relevant carbon observing system. *Biogeosciences* 11: 3547–3602.
- Damm A, Guanter L, Paul-Limoges E, van der Tol C, Hueni A, Buchmann N, Eugster W, Ammann C, Schaepman ME. 2015. Far-red sun-induced chlorophyll fluorescence shows ecosystem-specific relationships to gross primary production: An assessment based on observational and modeling approaches. *Remote Sensing of Environment* 166: 91–105.
- Demmig-Adams B, Garab G, Adams III W, Govindjee, Eds. 2014. "Non-Photochemical Quenching and Energy Dissipation" in Plants, Algae and Cyanobacteria (Springer, Dordrecht).
  - **Detto M, Xu X. 2020.** Optimal leaf life strategies determine  $V_{\rm cmax}$  dynamic during ontogeny. *New Phytologist* **228:** 361–375.
- Farquhar GD, von Caemmerer S, Berry JA. 1980. A biochemical model of photosynthetic CO<sub>2</sub> assimilation in leaves of C3 species. *Planta* 149: 78–90.
  - **Field C, Mooney HA. 1986.** The photosynthesis-nitrogen relationship in wild plants. In: Givnish T, eds. *On the Economy of Plant Form and Function*. Cambridge University Press, 25-55.
  - **Frankenberg C, Fisher JB, Worden J. 2011.** New global observations of the terrestrial carbon cycle from GOSAT: Patterns of plant fluorescence with gross primary productivity. *Geophysical Research Letters* **38:** L17706.
  - Gu L, Han J, Wood JD, Chang CY, Sun Y. 2019. Sun-induced Chl fluorescence and its

- importance for biophysical modeling of photosynthesis based on light reactions. *New Phytologist* **223**: 1179–1191.
- Gu L, Pallardy SG, Tu K, Law BE, Wullschleger SD. 2010. Reliable estimation of biochemical parameters from C3 leaf photosynthesis-intercellular carbon dioxide response curves. *Plant, Cell and Environment* 33: 1852–1874.

10

15

20

- Guanter L, Frankenberg C, Dudhia A, Lewis PE, Gómez-Dans J, Kuze A, Suto H, Grainger RG. 2012. Retrieval and global assessment of terrestrial chlorophyll fluorescence from GOSAT space measurements. *Remote Sensing of Environment* 121: 236–251.
- Guanter L, Zhang Y, Jung M, Joiner J, Voigt M, Berry JA, Frankenberg C, Huete AR, Zarco-Tejada P, Lee JE et al. 2014. Global and time-resolved monitoring of crop photosynthesis with chlorophyll fluorescence. In: Proceedings of the National Academy of *Sciences* 111: E1327–E1333.
- He L, Magney T, Dutta D, Yin Y, Köhler P, Grossmann K, Stutz J, Dold C, Hatfield J, Guan K, Peng B, Frankenberg C. 2020. From the ground to space: using solar-induced chlorophyll fluorescence to estimate crop productivity. *Geophysical Research Letters* 47: e2020GL087474.
- **Jiang C, Ryu Y. 2016.** Multi-scale evaluation of global gross primary productivity and evapotranspiration products derived from Breathing Earth System Simulator (BESS). *Remote Sensing of Environment* **186:** 528–547.
- **Johnson JE, Berry JA. 2021.** The role of Cytochrome b6f in the control of steady-state photosynthesis: a conceptual and quantitative model. *Photosynthesis Research* **148:** 101–136.
- Joiner J, Yoshida Y, Vasilkov A, Schaefer K, Jung M, Guanter L, Zhang Y, Garrity S, Middleton EM, Huemmrich KF et al. 2014. The seasonal cycle of satellite chlorophyll fluorescence observations and its relationship to vegetation phenology and ecosystem atmosphere carbon exchange. *Remote Sensing of Environment* 152: 375–391.
- Kattge J, Bönisch G, Díaz S, Lavorel S, Prentice IC, Leadley P, Tautenhahn S, Werner GDA, Aakala T, Abedi M et al. 2020. TRY plant trait database enhanced coverage and open

access. Global Change Biology 26: 119-188.

10

15

- Kattge J, Diaz S, Lavorel S, Prentice IC, Leadley P, Bönisch G, Garnier E, Westoby M, Reich PB, Wright IJ et al. 2011. TRY--a global database of plant traits. *Global Change Biology* 17: 2905–2935.
- Kattge J, Knorr W, Raddatz T, Wirth C. 2009. Quantifying photosynthetic capacity and its relationship to leaf nitrogen content for global scale terrestrial biosphere models. *Global Change Biology* 15: 976–991.
  - Keenan TF, Prentice IC, Canadell JG, Williams CA, Wang H, Raupach M, Collatz GJ. 2016.

    Recent pause in the growth rate of atmospheric CO<sub>2</sub> due to enhanced terrestrial carbon uptake.

    Nature Communications 7: 13428.
  - Keenan TF, Migliavacca M, Papale D, Baldocchi D, Reichestein M, Torn M, Wutzler T. 2019. Widespread inhibition of daytime ecosystem respiration. *Nature Ecology and Evolution* 3: 407–415.
  - Kira O, Chang CY-Y, Gu L, Wen J, Hong Z, Sun Y. 2021. Partitioning net ecosystem exchange (NEE) of CO2 using solar-induced chlorophyll fluorescence (SIF). *Geophysical Research Letters* 48: e2020GL091247.
    - **Koffi E, Rayner P, Norton A, Frankenberg C, Scholze M. 2015.** Investigating the usefulness of satellite derived fluorescence data in inferring gross primary productivity within the carbon cycle data assimilation system. *Biogeosciences Discussions* **12:** 707–749.
- 20 Kromdijk J, Głowacka K, Leonelli L, Gabilly ST, Iwai M, Krishna K, Niyogi KK, Long S P.
  2016. Improving photosynthesis and crop productivity by accelerating recovery from photoprotection. *Science* 354, 857-861.
  - Li X, Xiao J, He B, Altaf Arain M, Beringer J, Desai AR, Emmel C, Hollinger DY, Krasnova A, Mammarella I et al. 2018. Solar-induced chlorophyll fluorescence is strongly correlated with terrestrial photosynthesis for a wide variety of biomes: First global analysis based on OCO-2 and flux tower observations. *Global Change Biology* 24: 3990–4008.

- Liu L, Guan L, Liu X. 2017. Directly estimating diurnal changes in GPP for C3 and C4 crops using far-red sun-induced chlorophyll fluorescence. *Agricultural and Forest Meteorology* 232: 1–9.
- Liu X, Guanter L, Liu L, Damm A, Malenovský Z, Rascher U, Peng D, Du S, Gastellu-Etchegorry J. 2019. Downscaling of solar-induced chlorophyll fluorescence from canopy level to photosystem level using a random forest model. *Remote Sensing of Environment* 231: 110772.

15

20

- Magney TS, Barnes ML, Yang X. 2020. On the covariation of chlorophyll fluorescence and photosynthesis across scales. *Geophysical Research Letters* 47: e2020GL091098.
- Magney TS, Bowling DR, Logan BA, Grossmann K, Stutz J, Blanken PD, Burns SP, Cheng R, Garcia MA, Köhler P et al. 2019a. Mechanistic evidence for tracking the seasonality of photosynthesis with solar-induced fluorescence. *Proceedings of the National Academy of Sciences of the United States of America* 116: 11640–11645.
  - Magney TS, Frankenberg C, Köhler P, North G, Davis TS, Dold C, Dutta D, Fisher JB, Grossmann K, Harrington A et al. 2019b. Disentangling changes in the spectral shape of chlorophyll fluorescence: Implications for remote sensing of photosynthesis. *Journal of Geophysical Research: Biogeosciences* 124: 1491–1507.
  - Marrs JK, Reblin JS, Logan BA, Allen DW, Reinmann AB, Bombard DM, Tabachnik D, Hutyra LR. 2020. Solar-induced fluorescence does not track photosynthetic carbon assimilation following induced stomatal closure. *Geophysical Research Letters* 47: e02101.
  - Meeker EW, Magney TS, Bambach N, Momayyezi M, McElrone AJ. 2021. Modification of a gas exchange system to measure active and passive chlorophyll fluorescence simultaneously under field conditions. *AoB Plants* 13: plaa066.
  - Miao G, Guan K, Suyker AE, Yang X, Arkebauer TJ, Walter-Shea EA, Kimm H, Hmimina GY, Gamon JA, Franz TE et al. 2020. Varying contributions of drivers to the relationship between canopy photosynthesis and far-red sun-induced fluorescence for two maize sites at different temporal scales. *Journal of Geophysical Research: Biogeosciences* 125:

e2019JG005051.

5

10

15

- Miao G, Guan K, Yang X, Bernacchi CJ, Berry JA, DeLucia EH, Wu J, Moore CE, Meacham K, Cai Y et al. 2018. Sun-Induced chlorophyll fluorescence, photosynthesis, and light use efficiency of a soybean field from seasonally continuous measurements. *Journal of Geophysical Research: Biogeosciences* 123: 610–623.
- **Mohammed GH, Colombo R, Middleton EM. 2019.** Remote sensing of solar-induced chlorophyll fluorescence (SIF) in vegetation: 50 years of progress. *Remote Sensing of Environment* **231**: 111177.
- Nilkens M, Kress E, Lambrev P, Miloslavina Y, Müller M, Holzwarth AR, Jahns P. 2010. Identification of a slowly inducible zeaxanthin-dependent component of non-photochemical quenching of chlorophyll fluorescence generated under steady-state conditions in Arabidopsis. *Biochimica et Biophysica Acta (BBA) Bioenergetics* 1797: 466–475.
- **Norton AJ, Rayner PJ, Koffi EN, Scholze M, Silver JD, Wang YP. 2019.** Estimating global gross primary productivity using chlorophyll fluorescence and a data assimilation system with the BETHY-SCOPE model. *Biogeosciences* **16:** 3069–3093.
- **Oxborough K, Baker NR. 1997.** Resolving chlorophyll a fluorescence images of photosynthetic efficiency into photochemical and non-photochemical components calculation of qP and Fv'/Fm' without measuring Fo'. *Photosynthesis Research* **54:** 135–142.
- Parazoo NC, Magney T, Norton A, Raczka B, Bacour C, Maignan F, Baker I, Zhang YG, Qiu B, Shi M et al. 2020. Wide discrepancies in the magnitude and direction of modeled solar-induced chlorophyll fluorescence in response to light conditions. *Biogeosciences* 17: 3733–3755.
- **Pfündel E. 1998.** Estimating the contribution of Photosystem I to total leaf chlorophyll fluorescence. *Photosynthesis Research* **56:** 185–195.
- Porcar-Castell A, Tyystjärvi E, Atherton J, van der Tol C, Flexas J, Pfündel EE, Moreno J, Frankenberg C, Berry JA. 2014. Linking chlorophyll a fluorescence to photosynthesis for remote sensing applications: mechanisms and challenges. *Journal of Experimental Botany* 65:

15

20

- Porcar-Castell A, Malenovský Z, Magney T, Van Wittenberghe S, Fernández-Marín B, Maignan F, Zhang Y, Maseyk K, Atherton J, Albert LP et al. 2021. Chlorophyll a fluorescence illuminates a path connecting plant molecular biology to Earth-system science. *Nature Plants* 7: 998–1009.
- Raczka B, Porcar-Castell A, Magney T, Lee JE, Köhler P, Frankenberg C, Grossmann K, Logan BA, Stutz J, Blanken PD et al. 2019. Sustained nonphotochemical quenching shapes the seasonal pattern of solar-induced fluorescence at a High-elevation evergreen forest. *Journal of Geophysical Research: Biogeosciences* 124: 2005–2020.
- Roach T, Krieger-Liszkay A. 2014. Regulation of photosynthetic electron transport and photoinhibition. *Current Protein Peptide Science* 15: 351–362.
  - **Rochaix JD. 2011.** Regulation of photosynthetic electron transport. *Biochimica et Biophysica Acta* **1807:** 375–383.
  - Rogers A, Medlyn BE, Dukes JS, Bonan G, von Caemmerer S, Dietze MC, Kattge J, Leakey ADB, Mercado LM, Niinemets Ü et al. 2017. A roadmap for improving the representation of photosynthesis in Earth system models. *New Phytologist* 213: 22–42.
    - Rossini M, Meroni M, Migliavacca M, Manca G, Cogliati S, Busetto L, Picchi V, Cescatti A, Seufert G, Colombo R. 2010. High resolution field spectroscopy measurements for estimating gross ecosystem production in a rice field. *Agricultural and Forest Meteorology* 150: 1283–1296.
    - **Ruban AV. 2016.** Nonphotochemical chlorophyll fluorescence quenching: Mechanism and effectiveness in protecting plants from photodamage. *Plant Physiology* **170**: 1903–1916.
    - Ryu Y, Baldocchi DD, Kobayashi H, van Ingen C, Li J, Andy Black T, Beringer J, Gorsel E, Knohl A, Law BE, Roupsard O. 2011. Integration of MODIS land and atmosphere products with a coupled-process model to estimate gross primary productivity and evapotranspiration from 1 km to global scales. *Global Biogeochemical Cycles* 25: GB4017.

- Schaefer K, Schwalm CR, Williams C, Arain MA, Barr A, Chen JM, Davis KJ, Dimitrov D, Hilton TW, Hollinger DY et al. 2012. A model-data comparison of gross primary productivity: Results from the North American Carbon Program site synthesis. *Journal of Geophysical Research: Biogeosciences* 117: G03010.
- 5 **Schimel DS. 1995.** Terrestrial ecosystems and carbon cycle. *Global Change Biology* 1: 77-91.
  - **Schreiber U. 2004.** Pulse-Amplitude-Modulation (PAM) Fluorometry and Saturation Pulse Method: An Overview. In: Papageorgiou G.C., Govindjee (eds) Chlorophyll a Fluorescence. Advances in Photosynthesis and Respiration, Springer, Dordrecht, **19:** 279–319.
  - **Sharkey TD. 1985.** Photosynthesis in intact leaves of C3 plants: Physics, physiology and rate limitations. *The Botanical Review* **51:** 53–105.

15

- Sun Y, Frankenberg C, Wood JD, Schimel DS, Jung M, Guanter L, Drewry DT, Verma M, Porcar-Castell A, Griffis TJ et al. 2017. OCO-2 advances photosynthesis observation from space via solar-induced chlorophyll fluorescence. *Science* 358: eaam5747.
- Ivanov AG, Sane PV, Zeinalov Y, Malmberg G, Gardestrom P, Huner NPA, Oquist G. 2001.

  Photosynthetic electron transport adjustments in overwintering Scots pine (*Pinus sylvestris*L.). Planta 213: 575–585.
- **Tesa M, Thomson S, Gakamsky A. 2018.** Temperature-dependent quantum yield of fluorescence from plant leaves. *Application notes in Edinburgh instruments*. AN P41.
- Thum T, Zaehle S, Köhler P, Aalto T, Aurela M, Guanter L, Kolari P, Laurila T, Lohila A, Magnani F et al. 2017. Modelling sun-induced fluorescence and photosynthesis with a land surface model at local and regional scales in northern Europe. *Biogeosciences* 14: 1969–1987.
- van der Tol C, Berry JA, Campbell PKE. 2014. Models of fluorescence and photosynthesis for interpreting measurements of solar-induced chlorophyll fluorescence. *Journal of Geophysical Research: Biogeosciences* 119: 2312–2327.
- Verma M, SchimelD, Evans B, Frankenberg C, Beringer J, Drewry DT, Magney T,

  Marang I, Hutley L, Moore C et al. 2017. Effect of environmental conditions on the

- relationship between solar-induced fluorescence and gross primary productivity at an OzFlux grassland site. *Journal of Geophysical Research: Biogeosciences* **122:** 716–733.
- Verrelst J, van der Tol C, Magnani F, Sabater N, Rivera JP, Mohammed G, Moreno J. 2016. Evaluating the predictive power of sun-induced chlorophyll fluorescence to estimate net photosynthesis of vegetation canopies: A scope modeling study. *Remote Sensing of Environment* 176: 139–151.

10

- **von Caemmerer S. 2000.** Biochemical Models of Leaf Photosynthesis (CSIRO Publishing, Collingwood, Australia).
- von Caemmerer S, Farquhar GD. 1981. Some relationships between the biochemistry of photosynthesis and the gas exchange of leaves. *Planta* 153: 376–387.
- Walker AP, Johnson AL, Rogers A, Anderson J, Bridges RA, Fisher RA, Lu D, Ricciuto DM, Serbin SP, Ye M. 2021. Multi-hypothesis comparison of Farquhar and Collatz photosynthesis models reveals the unexpected influence of empirical assumptions at leaf and global scales. *Global Change Biology* 27: 804–822.
- Walker AP, Quaife T, van Bodegom PM, De Kauwe MG, Keenan TF, Joiner J, Lomas MR, MacBean N, Xu C, Yang X et al. 2017. The impact of alternative trait-scaling hypotheses for the maximum photosynthetic carboxylation rate ( $V_{\rm cmax}$ ) on global gross primary production. New Phytologist 215: 1370–1386.
- Walker AP, Beckerman AP, Gu L, Kattge J, Cernusak LA, Domingues TF, Scales JC,
   Wohlfahrt G, Wullschleger SD, Woodward FI. 2014. The relationship of leaf photosynthetic traits V<sub>cmax</sub> and J<sub>max</sub> to leaf nitrogen, leaf phosphorus, and specific leaf area: a meta-analysis and modeling study. Ecology and Evolution 4: 3218–3235.
  - Wehr R, Munger JW, McManus JB, Nelson DD, Zahniser MS, Davidson EA, Wofsy SC, Saleska SR. 2016. Seasonality of temperate forest photosynthesis and daytime respiration. *Nature* 534: 680–683.
  - **Wohlfahrt G, Gu L. 2015.** The many meanings of gross photosynthesis and their implication for photosynthesis research from leaf to globe. *Plant, Cell and Environment* **38:** 2500–2507.

- Wood JD, Griffis TJ, Baker JM, Frankenberg C, Verma M, Yuen K. 2017. Multiscale analyses of solar-induced florescence and gross primary production. *Geophysical Research Letters* 44: 533–541.
- **Wullschleger SD. 1993.** Biochemical limitations to carbon assimilation in C3 plants a retrospective analysis of the A/Ci curves from 109 species. *Journal of Experimental Botany* **44:** 907–920.

10

15

20

- Yang K, Ryu Y, Dechant B, Berry JA, Hwang Y, Jiang C, Kang M, Kim J, Kimm H, Kornfeld A, Yang X. 2018. Sun-induced chlorophyll fluorescence is more strongly related to absorbed light than to photosynthesis at half-hourly resolution in a rice paddy. *Remote Sensing of Environment* 216: 658–673.
- Yang P, van der Tol C. 2018. Linking canopy scattering of far-red sun-induced chlorophyll fluorescence with reflectance. *Remote Sensing of Environment* 209: 456–467.
- Yang P, van der Tol C, Campbell PKE, Middleton EM. 2021. Unraveling the physical and physiological basis for the solar-induced chlorophyll fluorescence and photosynthesis relationship using continuous leaf and canopy measurements of a corn crop. *Biogeosciences* 18: 441–465.
- Yang X, Tang J, Mustard JF, Lee J, Rossini M, Joiner J, Munger WJ, Kornfeld A, Richardson AD. 2015. Solar-induced chlorophyll fluorescence that correlates with canopy photosynthesis on diurnal and seasonal scales in a temperate deciduous forest. *Geophysical Research Letters* 42: 2977–2987.
- **Zaks J, Amarnath K, Kramer DM, Niyogi KK, Fleming GR. 2012.** A kinetic model of rapidly reversible nonphotochemical quenching. *PNAS* **109**: 15757-15762.
- **Zarco-Tejada PJ, Catalina A, González MR, Martín P. 2013a.** Relationships between net photosynthesis and steady-state chlorophyll fluorescence retrieved from airborne hyperspectral imagery. *Remote Sensing of Environment* **136:** 247–258.
- Zarco-Tejada PJ, Morales A, Testi L, Villalobos FJ. 2013b. Spatio-temporal patterns of chlorophyll fluorescence and physiological and structural indices acquired from

- hyperspectral imagery as compared with carbon fluxes measured with eddy covariance. *Remote Sensing of Environment* **133:** 102–115.
- Zhang Y, Guanter L, Berry JA, van der Tol C, Yang X, Tang J, Zhang F. 2016. Model-based analysis of the relationship between sun-induced chlorophyll fluorescence and gross primary production for remote sensing applications. *Remote Sensing of Environment* 187: 145–155.

- Zhang Y, Guanter L, Berry JA, Joiner J, van der Tol C, Huete A, Gitelson A, Voigt M, Kohler P. 2014. Estimation of vegetation photosynthetic capacity from space-based measurements of chlorophyll fluorescence for terrestrial biosphere models. *Global Change Biology* 20: 3727–3742.
- Zhu XG, Ort DR, Whitmarsh J, Long SP. 2004. The slow reversibility of photosystem II thermal energy dissipation on transfer from high to low light may cause large losses in carbon gain by crop canopies: a theoretical analysis. *Journal of Experimental Botany* 55: 1167–1175.
- Zeng Y, Badgley G, Dechant B, Ryu Y, Chen M, Berry JA. 2019. A practical approach for estimating the escape ratio of near-infrared solar-induced chlorophyll fluorescence. *Remote Sensing of Environment* 232: 111209.

## **Supporting Information**

5

10

- **Fig. S1** The relationships between the theoretical  $SIF_{PSII}$  and the  $SIF_{abaxial}$  measured with a modified LI-6800 coupled with a VIS-NIR FLAME Spectrometer.
- **Fig. S2** Comparison of  $q_L$  inferred from ChlF parameters vs estimated values using Eq. 5 for different PFTs.
- Fig. S3 Diagram of the parameter fitting and performance of MLR-SIF and FvCB.
- **Fig. S4** The assessment of the performance of MLR-SIF model using leave-one-out cross-validation for each species.
- **Fig. S5** The observed relationship of measured  $A_n$  with  $SIF_{PSII}$  for different plant species grouped by PFTs.
- **Fig. S6** The responses of  $q_L$  and NPQ to PAR for each PFT.
- Fig. S7 The relationships between measured  $A_n$  and  $q_L$  and NPQ, and between the modeled  $SIF_{PSII}$  and  $q_L$  and NPQ for  $C_3$  and  $C_4$  species.
- **Fig. S8** The impact of PFT-specificity of parameter values on the estimated  $A_n$  for different PFTs at the reference temperature 25 °C.
- **Fig. S9** The responses of measured  $A_n$  to  $C_i$  for different plant species grouped by PFTs.
- Fig. S10 The responses of  $SIF_{PSII}$  to  $C_i$  for different plant species grouped by PFTs.
- **Table S1** Description of plant species, the corresponding PFTs, their growth conditions, and specific measurement curves.
- Table S2 List of symbols and their definitions.
  - **Table S3** The fitted parameter values and statistics for each PFT in the MLR-SIF and FvCB models.
  - **Table S4** Description of plant species that used to concurrently measure PAM ChlF parameters and active ChlF spectral emission, and their growth and measurement conditions.
- Notes S1 Verification of the validity of the computed *SIF*<sub>PSII</sub> using the directly measured ChlF emission spectra
  - Notes S2 Plant growth environment
  - **Notes S3** Procedures for measuring light and CO<sub>2</sub> response curves, and  $F_{\rm m}$  and  $F_{\rm o}$
  - Notes S4 Data quality control
- Notes S5 Details of parameters fitting with FvCB